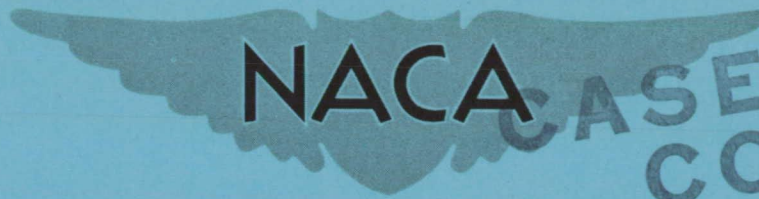


CONFIDENTIAL

Copy 346  
RM L51E14a



CASE FILE  
COPY

# RESEARCH MEMORANDUM

DIVISION OF LOAD AMONG THE WING, FUSELAGE,  
AND TAIL OF AIRCRAFT

By John P. Mayer and Clarence L. Gillis

Langley Aeronautical Laboratory  
Langley Field, Va.

CLASSIFICATION CHANGED TO UNCLASSIFIED  
AUTHORITY: NACA RESEARCH ABSTRACT NO. 127  
EFFECTIVE DATE: MAY 16, 1958  
WHL

This document contains classified information affecting the National Defense of the United States within the meaning of the Espionage Act, U.S.C. 1831 and 1832. Its transmission or the revelation of its contents in any manner to an unauthorized person is prohibited by law.

Information classified may be imparted only to persons in the military and naval services of the United States, contractors, agents, officers and employees of the Federal Government who have a legitimate interest therein, and to United States citizens of known loyalty and discretion who, in the interest of the Government, are deemed to be properly informed thereof.

## NATIONAL ADVISORY COMMITTEE FOR AERONAUTICS

WASHINGTON

May 29, 1951

CONFIDENTIAL

DECLASSIFIED

CONFIDENTIAL

NATIONAL ADVISORY COMMITTEE FOR AERONAUTICS

RESEARCH MEMORANDUM

DIVISION OF LOAD AMONG THE WING, FUSELAGE,  
AND TAIL OF AIRCRAFT

By John P. Mayer and Clarence L. Gillis

SUMMARY

Data are presented for the division of load among the wing, fuselage and tail for several aircraft configurations at subsonic and supersonic speeds. These data were obtained on full-scale airplanes, rocket-propelled models, and in low-speed wind-tunnel tests.

The data indicate that the component of total airplane load carried by the wing does not vary appreciably with Mach number for the full-scale airplanes.

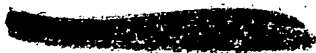
The present assumption that the fuselage carries load proportional to the area of the wing blanketed by the fuselage is shown to be roughly correct at low speeds and at supersonic speeds for the configurations tested.

In one series of wind-tunnel tests it is shown that wing incidence does not materially affect the component of additional load carried by the wing or fuselage.

The fuselage component of load becomes more predominant at high angles of attack for low-aspect-ratio wings.

INTRODUCTION

In the preliminary structural design of airplanes it has been the common assumption that the wing either carries all of the load or that the fuselage carries that portion of the load that would be carried by the intercepted wing area. Until recently, very little data have been available from the experimental sources that could be used to determine the division of load among the airplane components. In the past, wind-tunnel tests have consisted mostly of measurements of the lift of the



wing alone, the fuselage alone, and the wing-fuselage combination. In order to determine the division of load among the components, however, it is necessary to measure the wing loads in the presence of the fuselage. Recent advances in the measurement of wing and tail loads by means of strain gages have facilitated the measurement of component loads in flight. This paper presents some of the results obtained from full-scale flight tests and from rocket-propelled model tests at subsonic and supersonic speeds.


### SYMBOLS

$A_W$	exposed wing area, square feet
$A_{WF}$	total wing area, including portion blanketed by fuselage, square feet
$b$	wing span, feet
$c$	local wing chord, feet
$\bar{c}$	mean wing chord, feet
$c_l$	wing section lift coefficient
$C_L$	wing lift coefficient
$C_{N_A}$	airplane normal-force coefficient $\left( \frac{\text{Airplane normal force}}{qA_{WF}} \right)$
$C_{N_W}$	exposed wing component-normal-force coefficient $\left( \frac{\text{Wing normal force}}{qA_{WF}} \right)$
$C_{N_F}$	fuselage component-normal-force coefficient $\left( \frac{\text{Fuselage normal force}}{qA_{WF}} \right)$
$C_{N_T}$	horizontal tail-component normal-force coefficient $\left( \frac{\text{Tail normal force}}{qA_{WF}} \right)$
$C_{N_{WF}}$	wing-fuselage-component normal-force coefficient $\left( C_{N_W} + C_{N_F} \right)$

$C_{N_{W0}}$	wing-component normal-force coefficient at zero airplane normal-force coefficient
D	body diameter, feet
i	wing incidence, degrees
$L_W$	exposed wing load, pounds
M	Mach number
$n_W$	relative wing load factor $(L_W/W)$
q	dynamic pressure, pounds per square foot $(\frac{1}{2}\rho V^2)$
W	airplane weight, pounds
y	spanwise distance, feet
$\alpha$	angle of attack, degrees
$\delta$	stabilizer angle, degrees

#### METHODS

The component loads were measured on the full-scale airplanes by means of strain gages installed near the root stations of the wing and horizontal tail. Typical strain-gage locations and component-loads data for the full-scale investigations are presented in figure 1 for the Douglas D-558-II 35° swept-wing research airplane. (See reference 1.) The wing and tail loads were obtained from these strain-gage measurements and the airplane loads were obtained from a measurement of the normal acceleration at the airplane center of gravity and a knowledge of the weight of the airplane. The fuselage loads were determined indirectly by subtracting the sum of the wing and tail loads from the total airplane loads. All loads have been corrected for inertia effects and represent aerodynamic loads. The data are presented as plots of component normal-force coefficients based on the total wing area and the airplane normal-force coefficient. These data were obtained during gradual turns at Mach numbers of about 0.62 and 0.83 and are typical of the data obtained for all of the configurations tested. The slopes of the curves of wing and fuselage normal-force coefficient plotted against airplane normal-force coefficient represent the proportion of the total airplane lift caused by an angle-of-attack change that is being carried



CONFIDENTIAL

NACA RM L51E14a

by the individual components, or, in other words, the proportion of the additional lift carried by the components.

The component-loads data obtained by the use of free-flight rocket-propelled models were obtained from general research models differing only in wing plan form. The model configurations are shown in figure 2; one model has a  $60^\circ$  sweptback wing with an aspect ratio of 2.24 and the other has a  $45^\circ$  sweptback wing with an aspect ratio of 4. The  $60^\circ$  wing has a taper ratio of 0.33 and a thickness ratio of 0.055 at the root and 0.04 at the tip. The  $45^\circ$  wing has a taper ratio of 0.60 and a thickness ratio of 0.06. The wing normal force is measured by a beam balance, as shown in figure 2. The model contains a power system in the tail section to operate the all-movable elevator in a continuous square-wave motion during the flight. The data were obtained from analysis of the free oscillations which occur as a result of the abrupt elevator deflections. (See reference 2.) One model has also been flown without a wing to determine the tail effectiveness and the fuselage lift without any wing interference.

Typical normal-force data for a model incorporating the wing balance is shown in figure 3. These data were obtained on the model having a  $60^\circ$  swept wing. The plot shows wing normal-force coefficients plotted against total airplane normal-force coefficient. The data were obtained during the free oscillations of the model at fixed elevator deflections. Data are shown for elevator deflections of  $-1^\circ$  and  $2^\circ$  and at Mach numbers slightly less than 1.0. Similar data were obtained for the  $45^\circ$  swept wing except that lift coefficients of the order of 0.5 were attained. Again, the slopes of these curves represent the proportion of lift caused by an angle-of-attack change that is being carried by the exposed wing panels in the presence of the fuselage.

## RESULTS AND DISCUSSION

In figure 4 are shown the slopes of the component-load curves for three full-scale-airplane configurations as a function of Mach number. Flight data are presented for the unswept-wing Bell X-1 research airplane, the Douglas D-558-II swept-wing research airplane, and the North American B-45 jet-propelled bomber. It may be seen that the wing contribution does not vary appreciably with Mach number at Mach numbers up to about 1.2 for the X-1 airplane. Because of the rearward aerodynamic-center movement of the wing and fuselage, the tail component decreases with Mach number. The change in the contribution of the horizontal tail shown corresponds to a change in the wing-fuselage aerodynamic center of about 20 percent of the mean aerodynamic chord. This large change, however, does not appear as pronounced when viewed in terms of component

CONFIDENTIAL


loads. The contribution of the fuselage changes with Mach number to compensate for the change in the tail component with Mach number.

The contribution of the wing to the total airplane lift appears to remain approximately constant for the Mach number range shown for each of the other airplanes. The contribution of the tail and fuselage varies slightly with Mach number because of the movement of the wing-fuselage aerodynamic center with Mach number. In addition, the component of lift carried by the tail will change slightly with changes in the airplane center of gravity.

The slopes of the component-loads curves for the rocket models and the total-normal-force-curve slopes are shown in figure 5. Since the data were obtained during oscillations at fixed elevator settings the normal-force-curve slopes are untrimmed values and are shown as partial derivatives in contrast to the airplane data presented previously which involved trimmed normal-force data obtained in turns or pull-ups. For this reason the tail load that must be used to obtain fuselage loads for the rocket models is the rate of change of tail load with angle of attack at a fixed tail setting. The actual tail loads were not measured on the rocket models but the tail-lift effectiveness was measured. By use of this effectiveness and downwash values from transonic-bump tests and theoretical computations, the contribution of the tail to the untrimmed normal-force-curve slopes was determined. The resulting tail-, fuselage-, and wing-component-load-curve slopes are also shown in figure 5. Again the partial derivatives are used to indicate that angle of attack is the only variable. The model with the  $45^\circ$  swept wing exhibited a much greater normal-force-curve slope and a greater proportion of the total normal force carried by the wing than the model with the  $60^\circ$  swept wing. The difference is due to the larger aspect ratio and the larger ratio of exposed- to total-wing area of the  $45^\circ$  wing.

For both models the fuselage in the presence of the wing carried an appreciable proportion of the normal force. From the results of the test mentioned previously of this fuselage-tail configuration with no wing, the lift-curve slope of the fuselage alone was found to be very small, the magnitude approaching the order of accuracy of the data. Thus, the fuselage normal force shown here was practically all caused by the effect of the wing on the fuselage.

The variations of the component loads with Mach number for all of the configurations tested are shown in figure 6. In this figure the data are presented in terms of the wing-fuselage lift; the tail loads are not included. The slopes represent the proportion of wing-fuselage lift caused by an angle-of-attack change that is being carried by the wing and fuselage, respectively. Shown in figure 6 are data for the X-1, the B-45, and the D-558-II airplanes, the  $45^\circ$  rocket model, and the  $60^\circ$  rocket model.

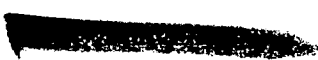


CONFIDENTIAL

It may be seen that in the subsonic region the component of lift carried by the wing or the fuselage is relatively constant with Mach number. In the transonic region the components vary somewhat with Mach number; however, from the results obtained thus far, there does not appear to be any consistent variation with Mach number among the configurations tested. At supersonic speeds, the data for the 60° model indicate that the wing component increases up to a Mach number of about 1.1 and then remains approximately constant at Mach numbers up to 1.55. The wing-component data for the 45° model do not change appreciably at Mach number up to about 1.28. The X-1 data indicate slight change in the wing component at supersonic speeds. It is of interest to note that, for the full-scale airplanes, the contribution of the wing to the total airplane lift did not vary appreciably with Mach number throughout the Mach number range.

In order to compare the experimental component-load results with those using methods of design, the experimental and calculated slopes of the wing-load-component curves at low lifts are shown in figure 7 for six airplane configurations. The methods used in obtaining the calculated results were the rough methods used in the past in which it was assumed that the fuselage carried that part of the load represented by the area intercepted by the fuselage. The span loadings for all of the airplanes were determined by lifting-line theory, and it was assumed that the wing extended to the airplane center line. The values of  $dC_{N_W}/dC_{N_{WF}}$  labeled "calculated" were obtained by taking the ratio of the portion of the span-loading diagram outboard of the wing-fuselage juncture to the total load. The values of  $dC_{N_W}/dC_{N_{WF}}$  labeled " $A_W/A_{WF}$ " are simply the ratio of the area of the wing outboard of the fuselage to the total wing area. The experimental values shown are given at low subsonic Mach numbers except for the two rocket models, where the experimental slopes are given at the highest supersonic Mach numbers. For the configurations tested thus far it is indicated that the wing-component load may be calculated at low speeds within about 5 percent by using the span-loading method or simply the area ratios. It is also indicated that, for the two rocket models tested, these rough rules are fairly good at supersonic speeds. At transonic speeds variations of the order of 10 to 15 percent are indicated for the configurations tested thus far.

In addition to the flight data shown here, some recent low-speed wind-tunnel data from the Ames Laboratory are of interest. Shown in figure 8 are data obtained for a wing having an aspect ratio of 3 combined with bodies of revolution having fineness ratios of 12.5. The component of lift carried by the wing is plotted against the ratio of the body diameter to the wing span. The data shown were obtained with wing incidences varying from 0° to 10° and at wing angles of attack up to 10°. It may be seen that wing incidences up to 10° have no apparent





effect on the component loads for these configurations. The calculated results obtained from the span-loading and area-ratio methods are also shown and are in fairly good agreement with the test data. The component of wing-fuselage lift carried by the wing, of course, decreases as the ratio of the body diameter to the wing span increases.

All of the data presented thus far have been for angle-of-attack and lift-coefficient ranges below the stall. Data obtained at angles of attack up to  $40^\circ$  for the D-558-II airplane are shown in figure 9. Shown in the upper part of the figure are the variations of the normal-force coefficients of the airplane, wing, fuselage, and horizontal tail with airplane angle of attack. (All of the normal-force coefficients are based on the total wing area.) It may be seen that the wing reaches a maximum normal force at an angle of attack of about  $22^\circ$ . The fuselage and tail normal-force coefficients, however, continue to increase throughout the angle-of-attack range and cause the airplane normal force to continue to increase. At the highest test angle of attack it can be seen that the fuselage normal force is almost as large as the wing normal force. The lower part of the figure is a plot of the ratio of the component normal-force coefficients to the airplane normal-force coefficient. The dashed lines indicate the value of the slope of the component-load curves for low normal coefficients. Again it may be seen that the component of load carried by the wing decreases at high angles of attack and that the component carried by the fuselage increases and is almost equal to that of the wing at the highest angle of attack.

The increase in the airplane normal-force coefficient due to the fuselage shown in figure 9 is not necessarily a phenomenon of swept wings but is more closely related to the ability of airplanes having low-aspect-ratio wings to reach high angles of attack. The aspect ratio of the D-558-II airplane is 3.57 and the sweep angle is  $35^\circ$ . The same characteristics might also be obtained with a low-aspect-ratio unswept-wing aircraft having a relatively large fuselage.

The increased normal force on the fuselage might be more correctly labeled as fuselage normal-drag component since at these high angles of attack the component of velocity across the fuselage becomes rather large and thus causes an increased normal force due to the drag normal to the fuselage.

Although it has been shown that wing incidence does not appreciably affect the additional component of lift caused by an angle-of-attack change, wing incidence may affect the absolute ratio of wing lift to the total airplane lift, especially at low lift coefficients. Shown in the upper part of figure 10 are the variations of the component normal-force coefficients with airplane normal-force coefficient at low normal-force coefficients for a typical airplane configuration. In regard to



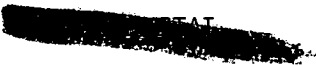
the structural design of an airplane when the magnitude of the over-all load is given by specification, the usual design assumptions will result in conservative designs for the wing over most of the normal-force-coefficient range. In the low normal-force-coefficient range, however, it may be seen that it is possible for the wing component to be greater than the airplane component, the extent depending on the zero-lift pitching-moment characteristics of the airplane. The value of  $C_{N_{W0}}$  is a measure of the zero-lift pitching-moment characteristics of the airplane. For instance, an airplane having a wing set at a large positive incidence relative to the fuselage might have a high value of  $C_{N_{W0}}$ .

For the airplanes for which test data are available, the zero-lift characteristics are such that the design load factor for the wing could not be reached at the airplane design load factor except at extremely high values of the dynamic pressure. For large airplanes, however, where the design load factors are low, it may be possible that the wing relative load factor could exceed the airplane design load factor in the normal speed range for the airplane. The variation of the relative load factor for the wing with dynamic pressure is shown in the lower part of figure 10 for an airplane having a wing loading of 50 and flying at its airplane design load factor of 3g. The solid line represents a zero-lift wing normal-force coefficient of 0.04 which is similar to one of the test configurations. The dashed line represents a zero-lift wing normal-force coefficient of 0.08 which might represent an airplane having a wing set at a fairly high incidence relative to the fuselage. The values of  $C_{N_{W0}}$  obtained for the airplanes tested thus far have ranged from

0.01 to 0.06. It may be seen for this configuration that very high dynamic pressures would have to be attained before the relative wing load factor would equal the airplane design load factor. For a value of  $C_{N_{W0}}$  of 0.04 the dynamic pressure at which the relative wing load

factor equals the airplane design load factor is about 770 pounds per square foot, which represents a sea-level speed of about 550 miles per hour. If the value of  $C_{N_{W0}}$  were doubled, the dynamic pressure at

which the two load factors were equal would decrease to about 370 pounds per square foot, which represents a sea-level speed of about 380 miles per hour. It appears, therefore, that the normal-force-coefficient range where the wing relative load factor would be greater than the airplane design load factor would be important only for unusual airplane configurations having high wing incidences and unusual zero-lift pitching-moment characteristics.



## CONCLUDING REMARKS

From the data presented previously the following general conclusions may be made. First, the component of total airplane load carried by the wing does not change appreciably with Mach number. Second, the present assumption that the fuselage carries load proportional to the area of the wing blanketed by the fuselage has been shown to be roughly correct at low speeds and at supersonic speeds for the configurations tested. Third, wing incidence has little effect on the component of additional load carried by the wing or fuselage for the low-aspect-ratio wing tested. Fourth, the fuselage component of load becomes more predominant at high angles of attack for low-aspect-ratio wings. Fifth, the normal-force-coefficient range where the wing would carry more than the total airplane load would be important only for airplane configurations having high wing incidences and unusual zero-lift pitching-moment characteristics.

Langley Aeronautical Laboratory  
National Advisory Committee for Aeronautics  
Langley Field, Va.

## REFERENCES

1. Mayer, John P., and Valentine, George M.: Flight Measurements with the Douglas D-558-II (BuAero No. 37974) Research Airplane. Measurements of the Distribution of the Aerodynamic Load among the Wing, Fuselage, and Horizontal Tail at Mach Numbers up to 0.87. NACA RM L50J13, 1951.
2. Gillis, Clarence L., Peck, Robert F., and Vitale, A. James: Preliminary Results from a Free-Flight Investigation at Transonic and Supersonic Speeds of the Longitudinal Stability and Control Characteristics of an Airplane Configuration with a Thin Straight Wing of Aspect Ratio 3. NACA RM L9K25a, 1950.

03172201030

CONFIDENTIAL

NACA RM L51E14a

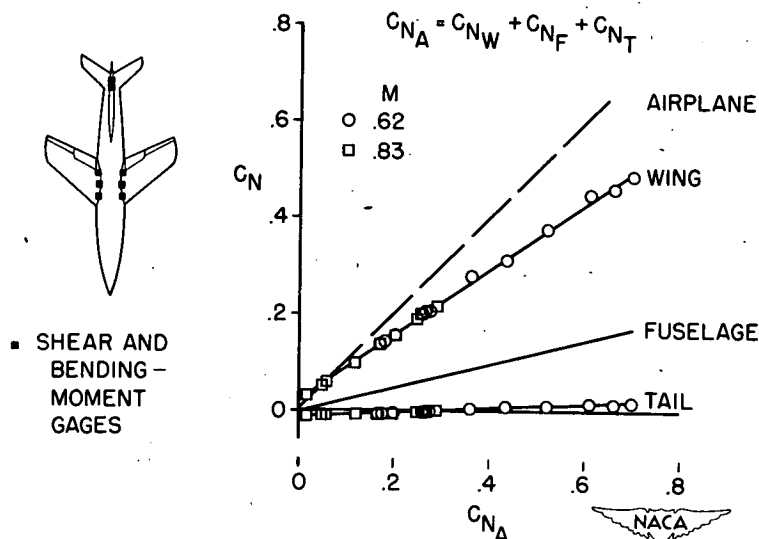


Figure 1.- Variation of component normal-force coefficients with airplane normal-force coefficient - D-558-II airplane.

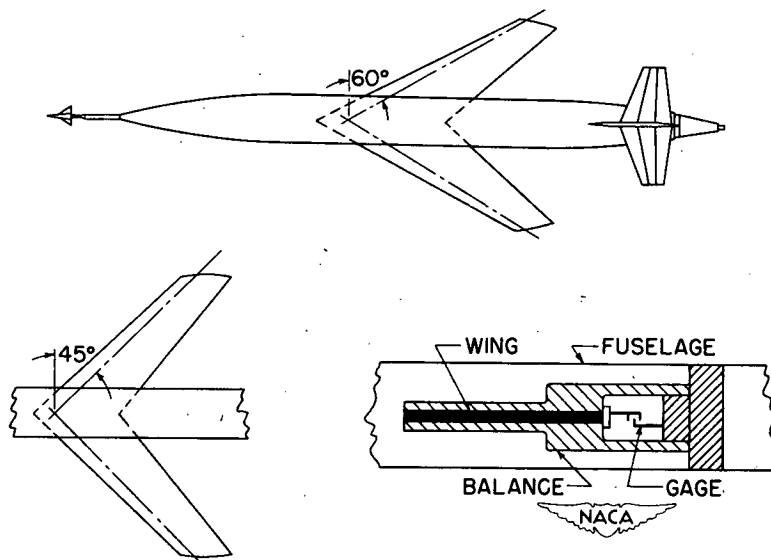


Figure 2.- Rocket-propelled model configurations and wing-lift balance.

D E C L A S S I F I E D  
 CONFIDENTIAL

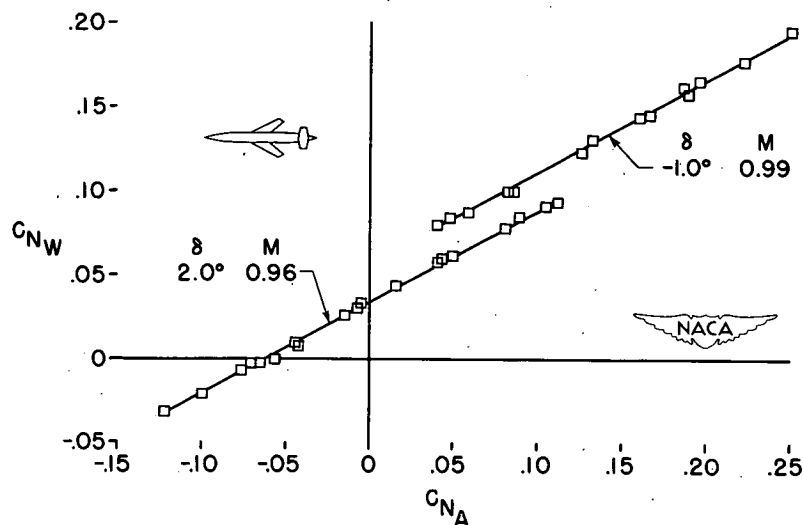


Figure 3.- Variation of wing-component normal-force coefficient with airplane normal-force coefficient ( $60^\circ$  swept-wing rocket model).

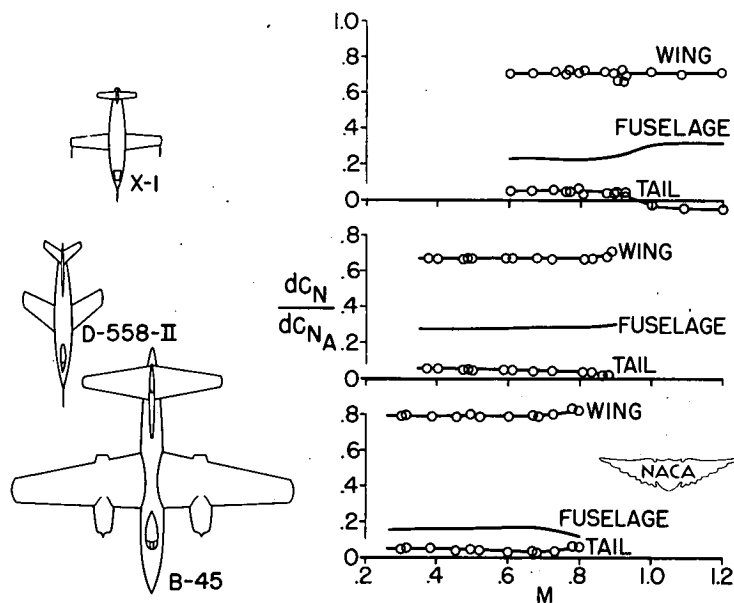


Figure 4.- Variation with Mach number of the component of additional load carried by the wing, fuselage, and horizontal tail for three airplane configurations.

03712201030

CONFIDENTIAL

NACA RM L51E14a

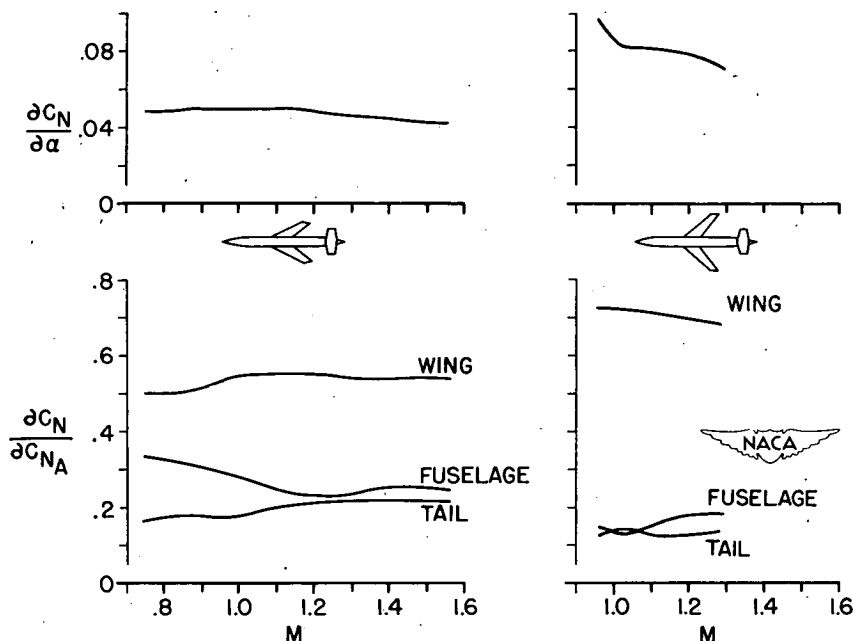


Figure 5.- Variation with Mach number of the lift-curve slopes and the components of additional load carried by the wing, fuselage, and horizontal tail for two rocket-propelled model configurations.

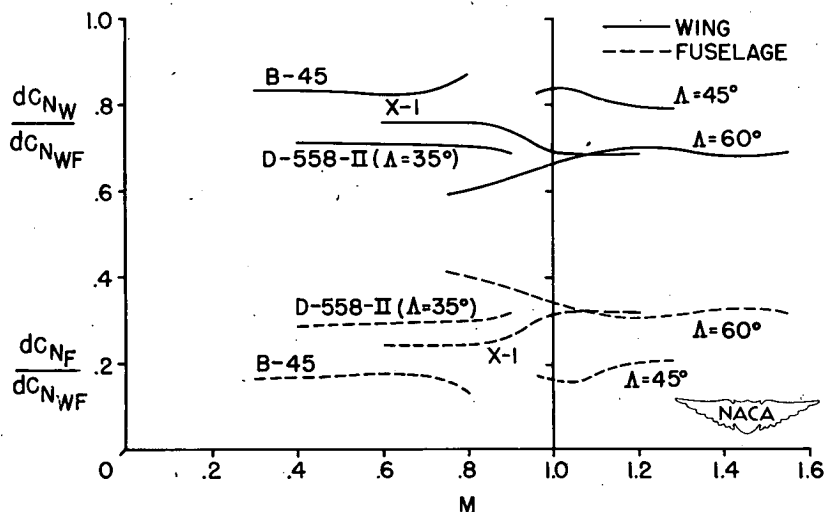


Figure 6.- Variation with Mach number of the component of additional wing-fuselage load carried by the wing and fuselage for several aircraft configurations.

DECLASSIFIED

CONFIDENTIAL

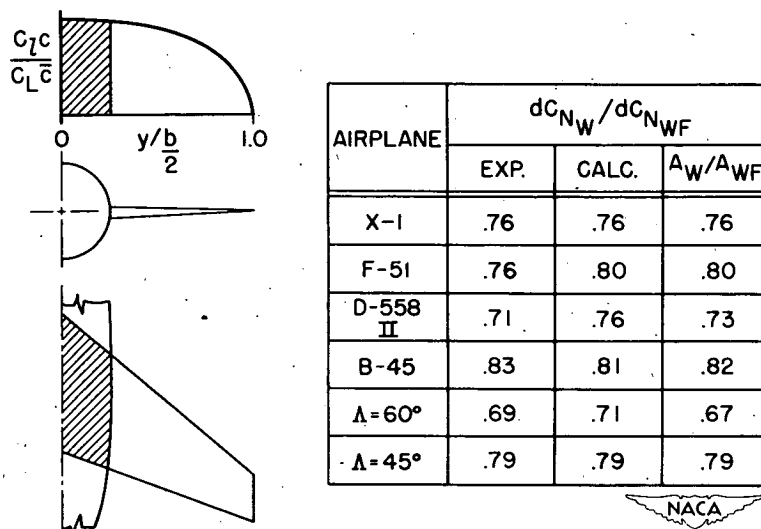


Figure 7.- Comparison between estimated and experimental components of load carried by the wing for several airplane configurations.

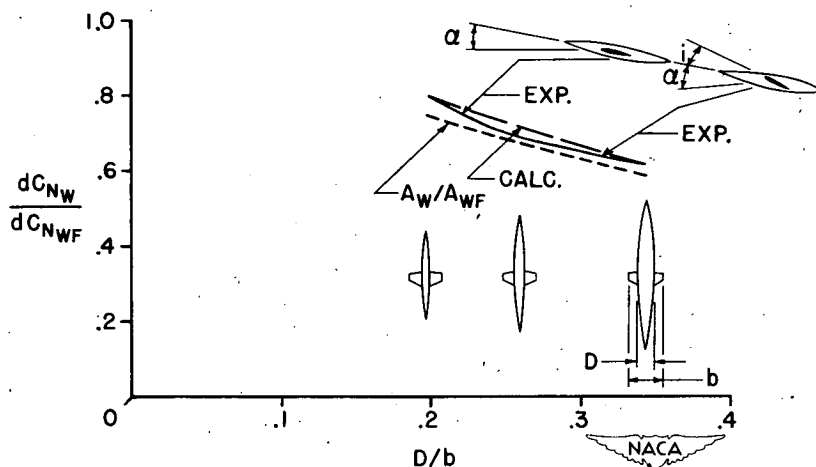


Figure 8.- Variation of the component of load carried by the wing with ratio of body diameter to wing span.

CONFIDENTIAL

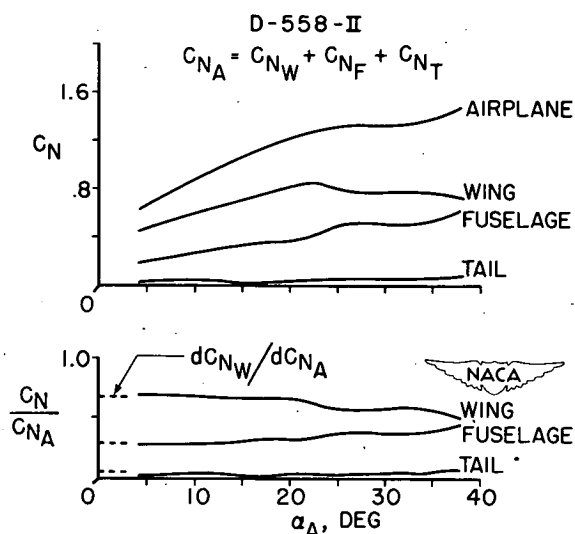


Figure 9.- Variation of the components of load carried by the wing, fuselage, and horizontal tail with angle of attack. (D-558-II airplane.)

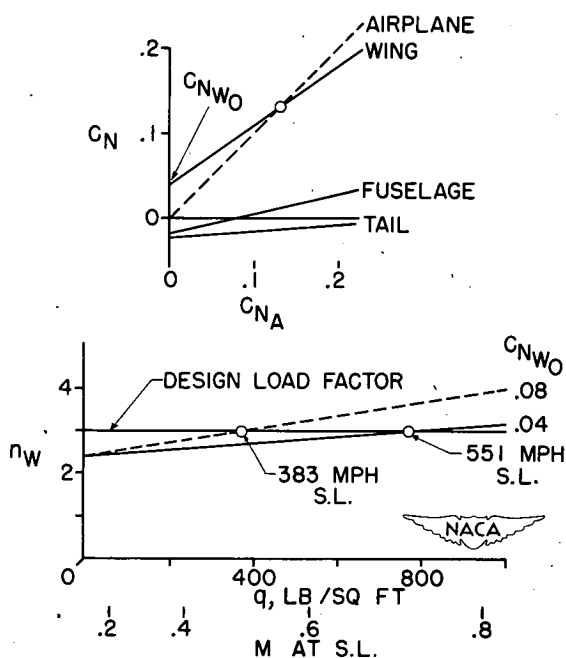


Figure 10.- Variation of the wing relative load factor with dynamic pressure for an airplane flying at its design load factor. ( $\frac{W}{S} = 50$ .)



DECLASSIFIED